# Supplementary Information to "Composite-pulse magnetometry with a solid-state quantum sensor"

Clarice D. Aiello, Masashi Hirose, and Paola Cappellaro*
*Department of Nuclear Science and Engineering,*
*Massachusetts Institute of Technology, Cambridge, MA 02139, USA*

## SUPPLEMENTARY FIGURES

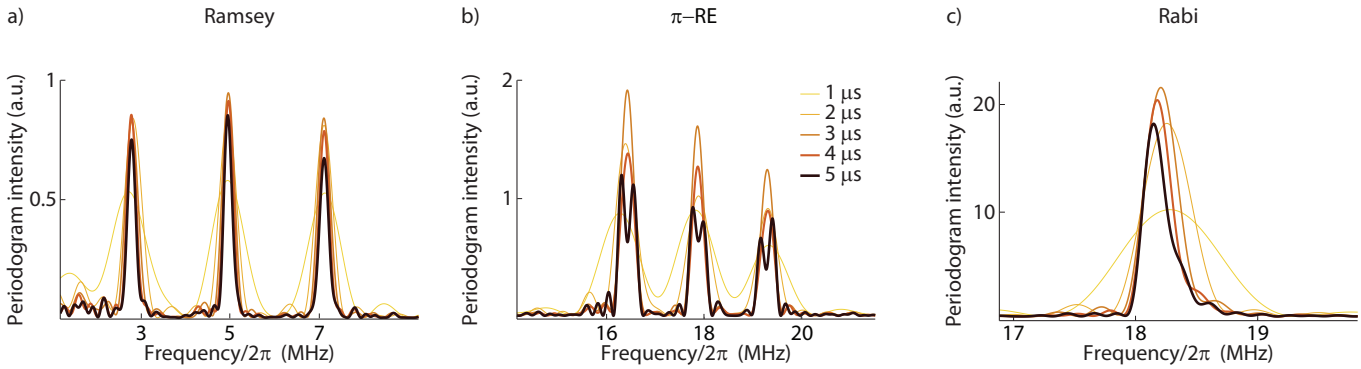


SUPPLEMENTARY FIG. S1. **Experimental periodograms for increasing interrogation times up to** $5\mu$**s.** a) Ramsey (5MHz detuned from the presumed resonance), b) $\pi$-rotary-echo and c) Rabi sequences. There is a trade-off between signal intensity and sensitivity to the detunings $\{b, A \pm b\}$ in the signal.

* pcappell@mit.edu

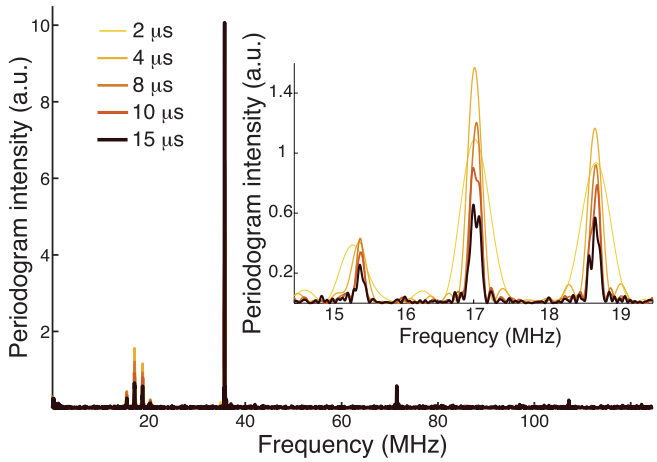


SUPPLEMENTARY FIG. S2. **Rotary-echo periodogram over the full spectrum.** Frequencies corresponding to the even harmonics of the Rabi frequency $\Omega$, which are present in the signal, but which are not contemplated by the first order of average Hamiltonian theory, can be clearly identified. In the inset, the signal peaks arising from the frequencies of interest are shown for interrogation times much longer than the dephasing time $T'_{\mathrm{RE}}$.

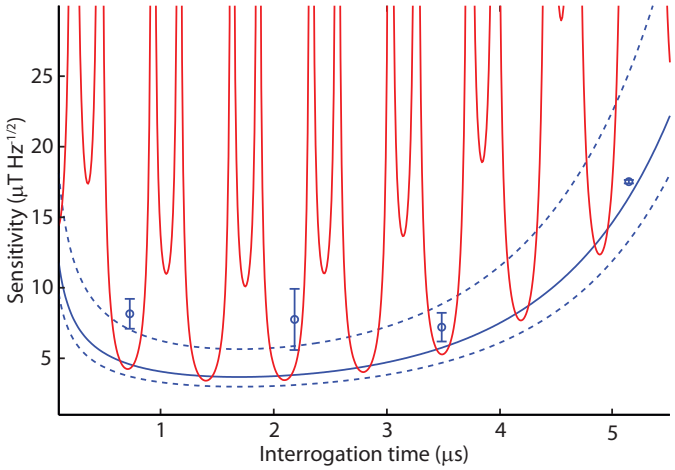


SUPPLEMENTARY FIG. S3. **Experimental sensitivity taking into account the time dependence of $\overline{C_A(t)}$.** This plot superimposes to Fig. 3 in the main text the expected sensitivity of the quantum magnetometer for all times of the correction factor $\overline{C \times C_A(t)}$ (solid red line). The experimental points (blue circles) are chosen accordingly, so as to have each one of the four realizations of $C_A$ at a local maximum. We see that the data do indeed correspond to points of maximal sensitivity of the quantum magnetometer. We note that the solid blue curve is estimated using an averaged correction factor $\overline{C \times C_A}$, for the four experimental realizations of $C$ and $C_A$.

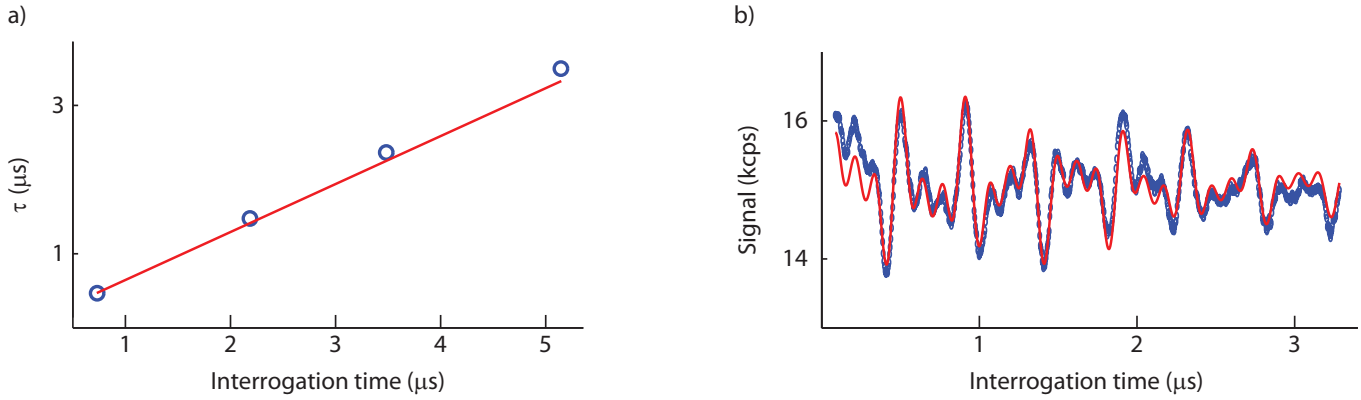


SUPPLEMENTARY FIG. S4. **Fitted parameters used to determine the experimental sensitivity.** a) The fitted periods $\tau$ (blue dots) are linear in the interrogation time $t$ and agree well with the theoretically expected time $2t\sin(\vartheta/2)/\vartheta$ (red line). b) The Ramsey signal (blue circles) is fitted to $\mathcal{S}_{\rm Ram} = k_1 - k_2\left[\cos(\delta\omega t) + \cos((A+\delta\omega)t) + \cos((A-\delta\omega)t)\right] e^{-(t/T_2^\star)^2}$ (red), with fitting parameters $\{k_1, k_2, \delta\omega, A, T_2^\star\}$. In particular, $T_2^\star \sim 2.19 \pm 0.15\mu$s.

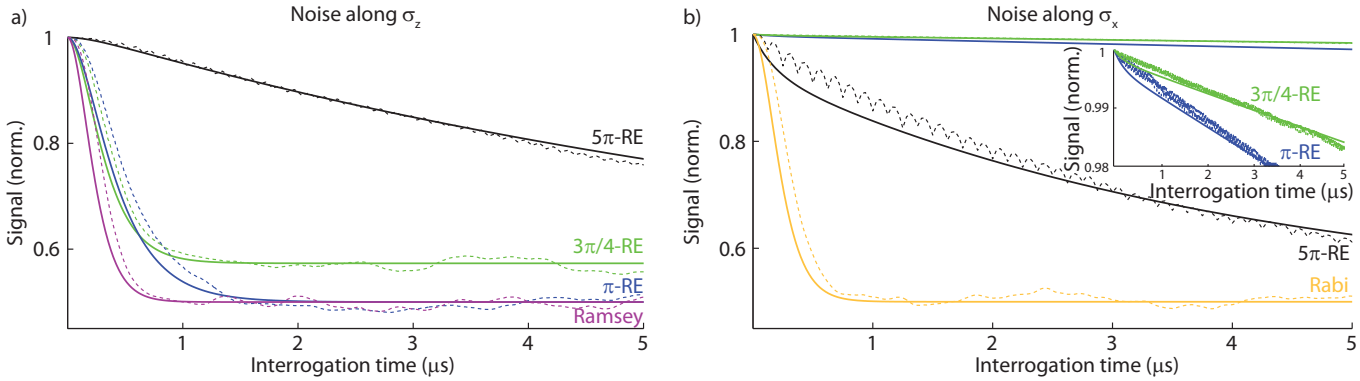


SUPPLEMENTARY FIG. S5. **Simulated signal decay in the presence of stochastic noise**. a) In the presence of stochastic bath noise, different $\vartheta$-RE with $\vartheta = \{3\pi/4, \pi, 5\pi\}$ (green, blue, black) are compared against a Ramsey sequence (purple); numerical simulations (dashed lines) agree with the formulas presented in the text (solid lines). The Ramsey sequence is the least resilient to bath noise, whereas one can adjust the dephasing of the RE by the choice of $\vartheta$; RE sequences are more resilient to bath noise with correlation times shorter than the echo period. The used numerical parameters are: $\Omega = 2\pi\times$20MHz, $\delta\omega = 2\pi\times$2MHz, $\tau_c = 200$ns, $\sigma = 0.05\Omega$. b) In the presence of stochastic noise in the excitation field, the situation is inverted: RE sequences refocus microwave noise with correlation times longer than the echo period; the decay of the Rabi sequence (orange) is plotted for comparison. Used parameters are the same as in a), except for $\delta\omega = 0$.

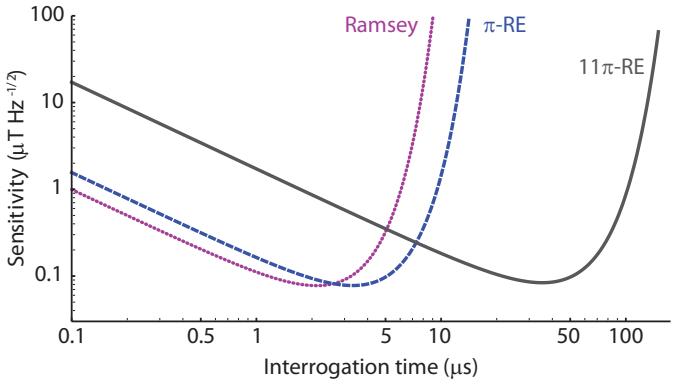


SUPPLEMENTARY FIG. S6. **Sensitivity with repeated readouts.** We compare the achievable sensitivity for Ramsey (purple, dotted) and rotary-echo ($\pi$-RE, blue, dashed; $11\pi$-RE, gray) sequences, when using the repeated readout scheme, with $N_{\rm r} = 100$ and the time per each readout $t_{\rm r} = 1.5\mu$s. In the presence of dephasing with $T_2^\star = 3\mu$s, the longer angle RE achieves good sensitivity for much longer interrogation times.

## SUPPLEMENTARY METHODS

### Dynamics under rotary-echo sequence

Consider a two-level system, $|0\rangle$ and $|1\rangle$, with resonance frequency $\omega_0$. The qubit is excited by radiation of frequency $\omega$ with associated Rabi frequency $\Omega$ and phase modulation $\varphi(t)$, such that the magnetic field amplitude is $\Omega\cos(\omega t+\varphi(t))$. The Hamiltonian is then

$$\mathcal{H}_{\rm lab}=\begin{pmatrix} 0 & \Omega\cos(\omega t+\varphi(t)) \\ \Omega\cos(\omega t+\varphi(t)) & \omega_0 \end{pmatrix} . \tag{S1}$$

In a frame rotating with the excitation field, the operator

$$U_{\rm rot}=\begin{pmatrix} 1 & 0 \\ 0 & e^{i\omega t} \end{pmatrix} \tag{S2}$$

transforms the Hamiltonian to

$$\mathcal{H}=\begin{pmatrix} 0 & \Omega\cos(\omega t+\varphi(t))e^{-i\omega t} \\ \Omega\cos(\omega t+\varphi(t))e^{i\omega t} & \omega_0-\omega \end{pmatrix} . \tag{S3}$$

Applying the rotating wave approximation and setting set $\delta\omega\equiv\omega_0-\omega$, the Hamiltonian reads

$$\mathcal{H}\approx\begin{pmatrix} 0 & \frac{\Omega}{2}e^{i\varphi(t)} \\ \frac{\Omega}{2}e^{-i\varphi(t)} & \delta\omega \end{pmatrix} . \tag{S4}$$

One rotary-echo (RE) is composed of two identical pulses of nominal rotation angle $\vartheta$ applied with excitation phases shifted by $\pi$. Under a sequence of RE, $e^{i\varphi(t)}=\mathbb{SW}(t)$, with $\mathbb{SW}(t)$ the square wave of period $T=\frac{2\vartheta}{\Omega}$ equal to the RE cycle time:

$$\mathbb{SW}(t)=\frac{4}{\pi}\sum_{k=1,\rm odd}^{\infty}\frac{1}{k}\sin\left(\frac{k\pi\Omega t}{\vartheta}\right) . \tag{S5}$$

On resonance ($\delta\omega=0$) the evolution operator is trivially obtained:

$$U_0=\begin{pmatrix} \cos(\frac{\Omega}{2}\mathbb{TW}(t)) & -i\sin(\frac{\Omega}{2}\mathbb{TW}(t)) \\ -i\sin(\frac{\Omega}{2}\mathbb{TW}(t)) & \cos(\frac{\Omega}{2}\mathbb{TW}(t)) \end{pmatrix}=\cos\left(\frac{\Omega}{2}\mathbb{TW}(t)\right)\mathbb{1}-i\sin\left(\frac{\Omega}{2}\mathbb{TW}(t)\right)\sigma_x , \tag{S6}$$

where $\mathbb{TW}(t)$ is the triangular wave representing the integral of $\mathbb{SW}(t)$,

$$\mathbb{TW}(t)=\frac{\vartheta}{2\Omega}-\frac{4\vartheta}{\pi^2\Omega}\sum_{k=1,\rm odd}^{\infty}\frac{1}{k^2}\cos\left(\frac{k\pi\Omega t}{\vartheta}\right) . \tag{S7}$$

Using $U_0$ we make a transformation to the toggling frame of the microwave [35] to obtain the Hamiltonian $\tilde{\mathcal{H}}$:

$$\tilde{\mathcal{H}}=\frac{\delta\omega}{2}\begin{pmatrix} 1-\cos(\Omega\mathbb{TW}(t)) & i\sin(\Omega\mathbb{TW}(t)) \\ -i\sin(\Omega\mathbb{TW}(t)) & 1+\cos(\Omega\mathbb{TW}(t)) \end{pmatrix}=\frac{\delta\omega}{2}\left[\mathbb{1}-\cos(\Omega\mathbb{TW}(t))\sigma_z-\sin(\Omega\mathbb{TW}(t))\sigma_y\right] . \tag{S8}$$

$\tilde{\mathcal{H}}$ is periodic with $T$ and has a strength $T\delta\omega\ll 1$, and can thus be analyzed with an average Hamiltonian expansion. In order to do so, we first express the elements of $\tilde{\mathcal{H}}$ in their Fourier series:

$$\cos(\Omega\mathbb{TW}(t))=\frac{\sin\vartheta}{\vartheta}+2\vartheta\sin\vartheta\sum_{k=1,\rm odd}^{\infty}\frac{(-1)^k}{\vartheta^2-k^2\pi^2}\cos\left(\frac{k\pi\Omega t}{\vartheta}\right) ; \tag{S9}$$

$$\sin(\Omega\mathbb{T}\mathbb{W}(t)) = \frac{1-\cos\vartheta}{\vartheta} + 2\vartheta \sum_{k=1,\text{odd}}^{\infty} \frac{(-1)^k((-1)^k - \cos\vartheta)}{\vartheta^2 - k^2\pi^2} \cos\left(\frac{k\pi\Omega t}{\vartheta}\right) . \tag{S10}$$

To first order then,

$$\overline{\mathcal{H}}^{(1)} = \frac{1}{T}\int_0^T \tilde{\mathcal{H}}(t')\mathrm{d}t' = \frac{\delta\omega}{\vartheta}\sin\left(\frac{\vartheta}{2}\right)\begin{pmatrix} -\cos(\vartheta/2) & i\sin(\vartheta/2) \\ -i\sin(\vartheta/2) & \cos(\vartheta/2) \end{pmatrix} = -\frac{\delta\omega}{\vartheta}\sin\left(\frac{\vartheta}{2}\right)\left[\cos\left(\frac{\vartheta}{2}\right)\sigma_z - \sin\left(\frac{\vartheta}{2}\right)\sigma_y\right] . \tag{S11}$$

For $n$ rotary cycles, the propagator is approximated by $U_{\mathrm{RE}} = e^{i\tilde{\mathcal{H}}(t)t} \approx e^{inT\overline{\mathcal{H}}^{(1)}}$. The population of a system initially prepared in $|0\rangle$, under the action of $U_{\mathrm{RE}}$, is described at full echo times by the signal

$$\mathcal{S}(n) \approx \frac{1}{2}\left[1 + \cos^2\left(\frac{\vartheta}{2}\right) + \sin^2\left(\frac{\vartheta}{2}\right)\cos\left(\frac{4\delta\omega n}{\Omega}\sin\left(\frac{\vartheta}{2}\right)\right)\right] . \tag{S12}$$

Extending the above approximation to include the fast Rabi-like oscillations of frequency $\frac{\pi\Omega}{(\vartheta \bmod 2\pi)}$, we obtain

$$\mathcal{S}(t) \approx \frac{1}{2}\left[1 + \cos^2\left(\frac{\vartheta}{2}\right) + \sin^2\left(\frac{\vartheta}{2}\right)\cos\left(\frac{2\delta\omega t}{\vartheta}\sin\left(\frac{\vartheta}{2}\right)\right)\cos\left(\frac{\pi\Omega t}{(\vartheta \bmod 2\pi)}\right)\right] , \tag{S13}$$

indicating the presence of two spectral lines at $\frac{\pi\Omega}{(\vartheta \bmod 2\pi)} \pm \frac{2\delta\omega}{\vartheta}\sin\left(\frac{\vartheta}{2}\right)$ for each existing detuning $\delta\omega$.

Our numerical studies suggest the existence of further signal components arising from higher frequency components in the Fourier expansion, which are not contemplated by the first-order approximation outlined above. Such components are $\propto \cos\left(\frac{2\delta\omega t}{\vartheta}\sin\left(\frac{\vartheta}{2}\right)\right)\cos\left(\frac{(2k+1)\pi\Omega t}{(\vartheta \bmod 2\pi)}\right)$ and $\propto \cos\left(\frac{2k\pi\Omega t}{(\vartheta \bmod 2\pi)}\right)$, $k \in \mathbb{Z}$, thus being linked to split pairs of spectral lines around $\frac{(2k+1)\pi\Omega t}{(\vartheta \bmod 2\pi)}$, and single lines at $\frac{2k\pi\Omega t}{(\vartheta \bmod 2\pi)}$.

## Rabi-beat magnetometry

Rabi-beat magnetometry using a single solid-state qubit was recently demonstrated [14]. The scheme presupposes the existence of an absolute frequency standard against which one wishes to resolve a nearby frequency. For magnetometry purposes then,

$$\mathcal{S} = \frac{1}{2}(\mathcal{S}_{\mathrm{Rabi}}(\delta\omega) - \mathcal{S}_{\mathrm{Rabi}}(0)) , \tag{S14}$$

where $\delta\omega$ denotes a detuning from the frequency standard. The sensitivity reads

$$\eta = \frac{1}{\gamma_{\mathrm{e}}}\lim_{\delta\omega\to 0}\frac{\Delta\mathcal{S}}{|\frac{\partial\mathcal{S}}{\partial\delta\omega}|}\sqrt{t} \approx \frac{\sqrt{2\Omega}}{\gamma_{\mathrm{e}}}\sqrt{\frac{t\Omega}{2 - 2\cos(t\Omega) - t\Omega\sin(t\Omega)}} ; \tag{S15}$$

$\eta$ is close to minima at $t \approx (2k + \frac{3}{2})\frac{\pi}{\Omega}$, yielding

$$\eta_{\min} \approx \frac{\sqrt{2\Omega}}{\gamma_e}\Big/\sqrt{1 + \frac{2}{t\Omega}} , \tag{S16}$$

which tends to $\sqrt{2\Omega}/\gamma_{\mathrm{e}}$ for increasingly large interrogation times.

## Periodogram

The periodogram is defined as the squared magnitude of the Fourier transform (FT) of the signal $\mathcal{S}(t)$ at times $t_j$ $(j = 1, \ldots, M)$, $\mathcal{P} \equiv \frac{1}{M}|\sum_{j=1}^{M} d_j e^{i\omega t_j}|^2$, where $d_j$ are the $M$ data points [36].

Unlike the FT, the periodogram does provide bounds for frequency estimation from spectral analysis, besides being able to accommodate for noise profiles beyond static and white noise [36]. Take a simple sinusoidal signal $d_t = K\cos(2\pi f t) + e_t$, where $e_t$ is the added noise characterized by a (least informative) Gaussian probability

distribution $\mathsf{Normal}(0,\sigma^2)$, with $\sigma$ in circular frequency units. To $\sigma$ is assigned Jeffrey's prior $\frac{1}{\sigma}$, which indicates complete ignorance of this scale parameter. Under these conditions, the estimate frequency content of the signal is given by $f_{\rm est} = f_{\rm peak} \pm \delta f$, where $f_{\rm peak}$ is the frequency of the periodogram peak, and

$$\delta f = \frac{2\sqrt{3}}{\pi} \frac{\sigma}{Kt\sqrt{M}} \ . \tag{S17}$$

Here $t$ is the total interrogation time for the $M$ data points. $\delta f$ correctly takes into account the effect of both the interrogation duration $t$ and the S/N $\equiv \frac{K_{\rm RMS}}{\sigma} = \frac{K}{\sqrt{2}\sigma}$, and is shown to correspond to the classical Cramer-Rao bound [37]. Note that $\delta f$ is in general smaller than the so-called Fourier limit, $\delta f_{\rm Fl} = \frac{1}{2t}$. The method is readily applicable to signals with multiple frequency content $\{f_i\}$.

In Supplementary Fig. S1, we compare typical experimental periodograms for $\pi$-RE, Ramsey and Rabi signals taken under the same conditions, for increasing interrogation times. The Ramsey periodogram, despite its lower signal intensity, clearly shows the 3 detunings $\{b + 2\pi\times 5\text{MHz}, A \pm (b + 2\pi\times 5\text{MHz})\}$ present in the signal after $1\mu$s; $\pi$-RE is sensitive to the residual detuning $b \sim 2\pi\times 0.17$MHz as explained in the main text after $5\mu$s; finally, the Rabi sequence would only become sensitive to $b$ after an interrogation time $\sim 188\mu$s, which is reflected in the broad single peak of the periodogram.

We estimate the statistical significance level $p$ of individual peaks [33]. Letting $I_m$ be the intensity of $m$-th largest ordinate among the total $M$ in the periodogram, and calculating

$$T_m = \frac{I_m}{\sum_k I_k - \sum_{l=1}^{m} I_l} \ , \tag{S18}$$

the statistical significance of the $m$-th peak $p_m$ is approximated by

$$p_m \approx (M - (m-1))(1 - T_m)^{M-m} \ . \tag{S19}$$

To determine $\delta f$, we first estimate the S/N for each periodogram peak by dividing the peak area by the noise floor below the line of $p = 0.01$.

The periodogram, if plotted over the full spectrum as in Supplementary Fig. S2, exhibits very high peaks corresponding to the even harmonics of $\Omega$ which are present in the signal, but which are not taken into account by the first order of average Hamiltonian theory. In the inset, the peak structure originated from the detunings of interest is plotted for times much longer than the dephasing time $T'_{\rm RE}$.

### Experimental sensitivity

For a fixed interrogation time $t$, and scanning the detuning from resonance $\delta\omega$, we expect to observe the signal

$$\mathcal{S}(\delta\omega) \propto \cos\left(\frac{2\delta\omega t}{\vartheta}\sin\left(\frac{\vartheta}{2}\right)\right) \equiv \cos\left(\delta\omega\tau\right) \ , \tag{S20}$$

with $\tau = \frac{2t}{\vartheta}\sin\left(\frac{\vartheta}{2}\right)$.

In every experimental run, reference curves are acquired along with the signal $\mathcal{S}$; they are noted $\mathcal{R}_0$ for the $|0\rangle$ state as obtained after laser polarization, and $\mathcal{R}_1$ for the $|1\rangle$ state as calibrated by adiabatic inversion. The signal is then normalized as

$$\overline{\mathcal{S}} = \frac{\mathcal{S} - \mathcal{R}_1}{\mathcal{R}_0 - \mathcal{R}_1} \ ; \tag{S21}$$

The standard deviation of the normalized signal is readily obtained

$$\Delta\overline{\mathcal{S}} = \sqrt{(\Delta\mathcal{R}_0)^2\left|\frac{\mathcal{S}-\mathcal{R}_1}{(\mathcal{R}_0-\mathcal{R}_1)^2}\right|^2 + (\Delta\mathcal{R}_1)^2\left|\frac{\mathcal{S}-\mathcal{R}_1}{(\mathcal{R}_0-\mathcal{R}_1)^2} - \frac{1}{\mathcal{R}_0-\mathcal{R}_1}\right|^2 + (\Delta\mathcal{S})^2\left|\frac{1}{\mathcal{R}_0-\mathcal{R}_1}\right|^2} \ . \tag{S22}$$

The sensitivity is calculated for the whole signal

$$\eta(\delta\omega) = \frac{1}{\gamma_e}\frac{\Delta\overline{\mathcal{S}}}{|\frac{\partial\overline{\mathcal{S}}}{\partial\delta\omega}|}\sqrt{Nt}\ ; \tag{S23}$$

for each fixed interrogation time $t$, we single out the minimum sensitivity $\eta(\delta\omega)$ within one period of the fitted oscillation period $\tau$, depicted in Supplementary Fig. S4.a.

The standard deviation for the sensitivity measurements is obtained by

$$\Delta\eta = \frac{1}{\gamma_e}\left|\frac{\partial\eta}{\partial\overline{\mathcal{S}}}\right|\Delta\overline{\mathcal{S}}\sqrt{Nt} = \frac{1}{\gamma_e}\left|\frac{1-2\overline{\mathcal{S}}}{2\sqrt{\overline{\mathcal{S}}(1-\overline{\mathcal{S}})}}\frac{1}{\frac{\partial\overline{\mathcal{S}}}{\partial\delta\omega}}\right|\Delta\overline{\mathcal{S}}\sqrt{Nt}\ . \tag{S24}$$

Additionally, to every point in the plot there corresponds a factor $C$ taking into account imperfect state detection [1, 38]. While the theoretical signal $\mathcal{S}$ represents the population in the $|0\rangle$ state, measured from the observable $M \equiv |0\rangle\langle 0|$, the experimental signal records photons emitted by both $|0\rangle$ and $|1\rangle$ states, so that the measurement operator is best experimentally described by $M' \equiv n_0|0\rangle\langle 0| + n_1|1\rangle\langle 1|$. Here, $\{n_0, n_1\}$ are Poisson-distributed variables that indicate the number of collected photons; if perfect state discrimination were possible, $n_0 \to \infty$ and $n_1 \to 0$. Including this effect, after $n$ full echo cycles, the signal is modified to

$$\mathcal{S}'(n) \approx \frac{1}{4}\left[(3n_0 + n_1 + (n_0 - n_1)\cos\vartheta) + (n_0 - n_1 - (n_0 - n_1)\cos\vartheta)\cos\left(\frac{4\delta\omega n}{\Omega}\sin\left(\frac{\vartheta}{2}\right)\right)\right]\ . \tag{S25}$$

We calculate the sensitivity for $\overline{\mathcal{S}'}$ in the best-case scenario of minimum sensitivity given by the accumulated phase $\left(\frac{4\delta\omega n}{\Omega}\sin\left(\frac{\vartheta}{2}\right)\right) = \frac{\pi}{2}$, and note the existence of a factor $C$, with respect to the ideal sensitivity, $\eta_{M'} = \eta_M/C$:

$$C^{-1} = \sqrt{1 + \frac{1}{2} + \frac{(-11n_0 + 5n_1)}{2(n_0 - n_1)^2} + \frac{\cos\vartheta}{2}\left(1 - \frac{(n_0 + n_1)}{(n_0 - n_1)^2}\right) + \frac{8n_0}{(n_0 - n_1)^2\sin^2(\vartheta/2)}}\ . \tag{S26}$$

We use for $n_0$ ($n_1$) the mean photon number for the $|0\rangle$ ($|1\rangle$) reference curve during each acquisition for different $t$. On average, $\overline{n_0} \sim 0.0022 \pm 0.0003$ and $\overline{n_1} \sim 0.0015 \pm 0.0002$.

We also consider the fact that the signal $\overline{\mathcal{S}'}$ has contributions from three detunings $\{\delta\omega, A \pm \delta\omega\}$, where $A$ is the hyperfine coupling between the NV center and spin-1 $^{14}$N nucleus; taking such detunings into account is, incidentally, fundamental for the choice of interrogation times: given the modulation imposed by the multiple frequencies in the signal, full echo times yielding a high signal amplitude are preferred. In order to compare the ideal sensitivity with the experimental one, in our experiments we need to introduce a further correction factor $C_A$, since the accumulated phase is only equal to the optimal $\frac{\pi}{2}$ for the experimental realizations with $m_I = 0$. We expect the sensitivity to become larger as $\eta_A = \eta_{M'}/C_A = \eta_M/(C \times C_A)$, with

$$C_A^{-1} = \frac{3}{\left|1 + 2\cos\left(\frac{2At\sin(\vartheta/2)}{\vartheta}\right)\right|}\ . \tag{S27}$$

In order to estimate $C \times C_A$, we use the fitted value for $A$ at each point ($\overline{A} \sim 2\pi \times (2.21 \pm 0.07)$MHz), the time $t$ corresponding to the number of cycles at which the experimental point was taken, and a corrected $\vartheta \sim 0.984\pi$ that takes into account the real angle, given the experimental Rabi frequency, imposed by the duration of the echo half cycle, which can be controlled only up to the inverse of the AWG sample rate. A mean total correction factor of $\overline{C \times C_A} \sim (5.9 \pm 1.4) \times 10^{-3}$ is obtained for the set of points. The mean sensitivity curve (solid line) is expressed as the theoretically expected sensitivity in the absence of noise $\eta_M$, divided by $\overline{C \times C_A}$. Similarly, the lower (higher) bounds for the sensitivity are estimated by dividing the theoretical sensitivity by the maximum (minimum) $C \times C_A$ value in the set of points, and are plotted in the dashed blue lines.

We stress that the presence of an unpolarized nitrogen nuclear spin is the sole responsible for the $C_A(t)$ factor. The experimental sensitivity points were thus chosen for times having $C_A(t)$ at a local maximum. The landscape of the quantum magnetometer's expected sensitivity as a function of interrogation time, for an averaged $\overline{C \times C_A(t)}$ that considers the time dependence of $\overline{C_A(t)}$, is shown in red in Supplementary Fig. S3. The data cover the interrogation times where the sensitivity is optimal, even if the effect of the nitrogen nuclear spin were to be corrected for. Polarizing

the nuclear spin [27] or decoupling it with a simple pulse sequence such as a spin echo [6] would remove the effects of the hyperfine coupling and thus set $C_A = 1$. In the experiments, given our careful choice of interrogation times and the estimated hyperfine interaction A, the average over the four points $\overline{C_A} \sim 0.90 \pm 0.13$ is very close to 1.

The effect of decoherence is included in the plot using a fit for $T_2^\star \sim 2.19 \pm 0.15\mu$s from the Ramsey experiment shown in Supplementary Fig. S4.b. Assuming static Gaussian noise, we let $\eta_A \to \eta_A e^{(t/T'_{\rm RE})^2}$, with $T'_{\rm RE} = \frac{T_2^\star \vartheta}{2\sin(\vartheta/2)}$.

### Evolution under bath noise

In the presence of Gaussian static noise in the $z$-direction with variance $\sigma^2$, the RE signal decays as

$$\langle \mathcal{S}_{\rm RE} \rangle = \frac{1}{2}\left[1 + \cos^2\left(\frac{\vartheta}{2}\right) + \sin^2\left(\frac{\vartheta}{2}\right)\cos\left(\frac{2\delta\omega t}{\vartheta}\sin\left(\frac{\vartheta}{2}\right)\right) e^{(t/T'_{\rm RE})^2}\right] , \tag{S28}$$

where we define the dephasing time

$$T'_{\rm RE} = \frac{\vartheta}{\sigma\sqrt{2}|\sin(\vartheta/2)|} . \tag{S29}$$

Similarly, one obtains for the Ramsey signal

$$\langle \mathcal{S}_{\rm Ram} \rangle = \frac{1}{2}\left(1 + \cos(\delta\omega t) e^{-(t/T'_{\rm Ram})^2}\right) , \quad \text{with} \quad T'_{\rm Ram} = T_2^\star = \frac{\sqrt{2}}{\sigma} . \tag{S30}$$

Note that $T'_{\rm RE} > T'_{\rm Ram}$ always; nevertheless, at the optimum interrogation time calculated for both sequences as $\frac{T'}{2}$,

$$\frac{\eta_{\rm RE}}{\eta_{\rm Ram}} = \sqrt{\frac{\vartheta}{2\sin(\vartheta/2)^3}} > 1 ; \tag{S31}$$

the sensitivity ratio above has a minimum $\eta_{\rm RE}/\eta_{\rm Ram} \sim 1.20$ for $\vartheta \sim \frac{3\pi}{4}$, which is the angle that yields the highest sensitivity for the RE sequence.

We now turn our attention to the evolution of the Rabi signal under Gaussian dephasing noise. For $\delta\omega \ll \Omega$, the Rabi signal is approximately

$$\mathcal{S}_{\rm Rabi} = 1 - \frac{\Omega^2}{\Omega^2 + \delta\omega^2}\sin^2\left(\frac{t}{2}\sqrt{\Omega^2 + \delta\omega^2}\right) \approx 1 - \left(1 - \frac{\delta\omega^2}{\Omega^2}\right)\sin^2\left(\frac{t}{2}\left(\Omega + \frac{\delta\omega^2}{\Omega}\right)\right) ; \tag{S32}$$

calculating the expected value $\langle \mathcal{S}_{\rm Rabi} \rangle$ under the noise distribution yields

$$\langle \mathcal{S}_{\rm Rabi} \rangle = \frac{1}{2}\left[1 + \frac{\cos(t\Omega + \arctan(t\sigma^2/\Omega)/2)}{\left(1 + \frac{t^2\sigma^4}{\Omega^2}\right)^{\frac{1}{4}}} + \frac{\sigma^2}{\Omega^2}\left(1 - \frac{\cos(t\Omega + 3\arctan(t\sigma^2/\Omega)/2)}{\left(1 + \frac{t^2\sigma^4}{\Omega^2}\right)^{\frac{3}{4}}}\right)\right] . \tag{S33}$$

In the presence of stochastic (Ornstein-Uhlenbeck) noise with zero mean and autocorrelation function $\sigma^2 e^{-\frac{t}{\tau_{\rm c}}}$, a Ramsey signal decays as [39]

$$\langle \mathcal{S}_{\rm Ram} \rangle = \frac{1}{2}\left(1 + e^{-\zeta'(t)}\right) , \quad \text{with} \quad \zeta'(t) = \sigma^2\tau_{\rm c}^2(t/\tau_{\rm c} + e^{-\frac{t}{\tau_{\rm c}}} - 1) . \tag{S34}$$

Numerical simulations valid for $\tau_{\rm c}\sigma \lesssim \vartheta/2$ and $\tau_{\rm c} \gtrsim \vartheta/(2\Omega)$ indicate that the RE signal decays as

$$\langle \mathcal{S}_{\rm RE} \rangle = \frac{1}{2}\left[1 + \cos^2\left(\frac{\vartheta}{2}\right) + \sin^2\left(\frac{\vartheta}{2}\right) e^{-\zeta(t)}\right] , \tag{S35}$$

with

$$\zeta(t) = \zeta'(t)\frac{4\sin^2(\vartheta/2)}{\vartheta^2} . \tag{S36}$$

Note the additional factor $\frac{4\sin^2(\vartheta/2)}{\vartheta^2} = \left(\frac{T'_{\rm Ram}}{T'_{\rm RE}}\right)^2 < 1$.

Simulations that compare different $\vartheta$-RE for $\vartheta = \{3\pi/4, \pi, 5\pi\}$ and Ramsey signals in the presence of stochastic noise are depicted in Supplementary Fig. S5.a; it is clear that RE sequences are more resilient to bath noise with correlation times shorter than the echo period.

Previous calculations [40] indicate that, for slow baths $\frac{1}{\tau_{\rm c}} \ll \frac{\sigma^2}{\Omega}$, the Rabi signal follows the static noise behaviour for short times, and decays $\propto e^{-\frac{\sigma t}{2\sqrt{\tau_{\rm c}\Omega}}}$ for long times. Fast baths $\frac{1}{\tau_{\rm c}} \gg \frac{\sigma^2}{\Omega}$ induce a decay of the Rabi signal $\propto e^{\frac{4\Omega^2}{\sigma^4\tau_{\rm c}}}$.

### Evolution under excitation field noise

In the presence of a constant error in the Rabi frequency such that $\Omega \to (1+\epsilon)\Omega$, the infidelity $(1-{\rm Tr}[U(\epsilon)U(0)]/2) \equiv (1-F)$ of the pulse sequence is given to second order in the detuning from resonance $\delta\omega$ and in $\epsilon$ by

$$(1-F)_{\rm RE} \approx \frac{\epsilon^2 t^2 \delta\omega^2}{8}\frac{(2+\vartheta^2-2\cos\vartheta-2\vartheta\sin\vartheta)}{\vartheta^2} \tag{S37}$$

for RE and

$$(1-F)_{\rm Rabi} \approx \frac{\epsilon^2 t^2\Omega^2}{8} - \frac{\epsilon^2\delta\omega^2(-2+t^2\Omega^2+2\cos(t\Omega))}{8\Omega^2} \tag{S38}$$

for Rabi-beat magnetometry.

Similarly, an error in the Rabi frequency will yield a flip-angle error in the Ramsey sequence, resulting in the infidelity

$$(1-F)_{\rm Ram} \approx \frac{\epsilon^2\pi^2}{8} - \frac{\epsilon^2\delta\omega^2(-16+4\pi^2+\pi t\Omega(8+\pi t\Omega))}{32\Omega^2}\ . \tag{S39}$$

In the presence of stochastic noise in the excitation field with zero mean and autocorrelation function $\sigma^2 e^{-\frac{t}{\tau_{\rm c}}}$, the resonant cases for RE, Rabi have simple analytical solutions.

A cumulant expansion technique applied to periodic Hamiltonians [39, 41] yields for the envelope of a resonant RE sequence

$$\langle \mathcal{S}_{\rm RE}\rangle = \frac{1}{2}\left(1+e^{-\zeta(n)}\right)\ , \tag{S40}$$

with

$$\zeta(n) = \tau_{\rm c}^2\sigma^2\left[\frac{2n\vartheta}{\sigma\tau_{\rm c}} + 2n(e^{-\frac{\vartheta}{\Omega\tau_{\rm c}}}-1) - \tanh^2\left(\frac{1}{2}\frac{\vartheta}{\Omega\tau_{\rm c}}\right)\left(2n(e^{-\frac{\vartheta}{\Omega\tau_{\rm c}}}+1)+e^{-\frac{2n\vartheta}{\tau_{\rm c}\sigma}}-1\right)\right]\ . \tag{S41}$$

We note that this decay is equivalent to the decay under pure dephasing for a PDD sequence [42].

In Supplementary Fig. S5.b, we simulate the signal for different $\vartheta$-RE and Rabi sequences if noise in the excitation field is present. Contrarily to RE decay in the presence of bath noise, and as shown experimentally in the main text, RE sequences can refocus excitation noise with correlation times longer than the echo period.

We note that the Rabi signal decay for noise along $\sigma_x$ should be comparable to Ramsey signal decay in the presence of stochastic noise along $\sigma_z$. We thus have the decay

$$\langle \mathcal{S}_{\rm Rabi}\rangle = \frac{1}{2}\left(1+e^{-\zeta'(t)}\right)\ ,\quad \text{with}\quad \zeta'(t) = \sigma^2\tau_{\rm c}^2(t/\tau_{\rm c}+e^{-\frac{t}{\tau_{\rm c}}}-1)\ . \tag{S42}$$

The advantage of the RE sequence over the Rabi is thus the same advantage that dynamical decoupling sequences can offer.

### Repeated readouts

The NV spin state can be read under non-resonant illumination at room temperature using the fact that the $m_S = \pm 1$ excited states can decay into metastable states, which live for ∼300 ns, while direct optical decay happens in about 12 ns. Thus, a NV in the $m_S = 0$ state will emit, and absorb, approximately 15 photons, compared to only a few for a NV in the $m_S = \pm 1$ states, yielding state discrimination by fluorescence intensity. Unfortunately the metastable state decays primarily via spin-non conserving processes into the $m_S = 0$ state thereby re-orienting the spin. This is good for spin polarization, but erases the spin memory and reduces measurement contrast. The detection efficiency $C$ of the NV center spin state is thus given by Eq. S26, which for $\vartheta = k\pi$ reduces to $C = \left(1 + \frac{3(n_0+n_1)}{(n_0-n_1)^2}\right)^{-1/2}$, where $n_{1,0}$ is the number of photons collected if the NV spin is in the $m_S = \{0, 1\}$ state, respectively.

In the repeated readout scheme [27, 43], the state of the nuclear spin is repetitively mapped onto the electronic spin, which is then read out under laser illumination. The measurement projects the nuclear spin state into a mixed state, but the information about its population difference is preserved, under the assumption that the measurement is a good quantum non-demolition measurement. We can include the effect of these repeated readout by defining a new detection efficiency, $C_{N_r} = \left(1 + \frac{1}{N_r}\frac{3(n_0+n_1)}{(n_0-n_1)^2}\right)^{-1/2}$, which shows an improvement $\propto \sqrt{N_r}$, where $N_r$ is the number of measurements. The sensitivity needs of course to be further modified to take into account the increased measurement time. Provided the time needed for one measurement step is smaller than the interrogation time, it becomes advantageous to use repeated readouts. As RE increases the interrogation time, it can achieve better sensitivity than Ramsey magnetometry by using the repeated readout scheme (which is instead not advantageous for a simple Ramsey scheme), as depicted in Supplementary Fig. S6.

### Calcium signaling domains

Although virtually all neuronal reactions are regulated by diffusing $Ca^{2+}$ ions between membrane channel sources and cytoplasm target receptors, triggering specificity is ensured by the fact that such diffusion events are localized in time and space. The size of the signaling domain, understood as roughly the distance between channel and receptor (50nm to 0.5$\mu$m), determines the diffusion timescale ($\mu$s to ms) and strength, the latter measured by $Ca^{2+}$ concentration (100 to 1$\mu$M) [29, 44].

Let a flux with duration $t$ and mean travelled distance $d$ between membrane channel and cytoplasm receptor. The magnetic field at a distance $r$ from a transient $Ca^{+2}$ flux composed of $l$ ions is estimated as

$$B(\mathrm{T}) = \frac{\mu_0}{4\pi}\frac{2led}{tr^2}\ , \tag{S43}$$

with $e$ the electron charge, and with the magnetic permeability of the cell approximated by $\mu_0$, the vacuum permeability. Therefore, the minimum required sensitivity to sense the afore-described calcium flux is

$$\eta\left(\frac{\mathrm{T}}{\sqrt{\mathrm{Hz}}}\right) = \sqrt{2\pi}\frac{\mu_0}{4\pi}\frac{2led}{\sqrt{t}r^2}\sqrt{N}\ . \tag{S44}$$

## SUPPLEMENTARY REFERENCES


[35] M. Duer, *Introduction to solid-state NMR spectroscopy* (John Wiley & Sons, 2004)

[36] G. L. Bretthorst, *Bayesian spectrum analysis and parameter estimation* (Springer-Verlag, 1988)

[37] D. C. Rife and R. R. Boorstyn, *Single tone parameter estimation from discrete-time observations.* IEEE Transactions on Information Theory **20**, 591–598 (1974)

[38] C. A. Meriles, L. Jiang, G. Goldstein, J. S. Hodges, J. Maze, M. D. Lukin, and P. Cappellaro, *Imaging mesoscopic nuclear spin noise with a diamond magnetometer.* J. Chem. Phys. **133**, 124105 (2010)

[39] R. Kubo, *Generalized cumulant expansion method.* J. Phys. Soc. Jpn. **17**, 1100–1120 (1962)

[40] V. V. Dobrovitski, A. E. Feiguin, R. Hanson, and D. D. Awschalom, *Decay of Rabi oscillations by dipolar-coupled dynamical spin environments.* Phys. Rev. Lett. **102**, 237601 (2009)

[41] P. Cappellaro, J. S. Hodges, T. F. Havel, and D. G. Cory, *Principles of control for decoherence-free subsystems.* J. Chem. Phys. **125**, 044514 (2006)

[42] K. Khodjasteh and D. A. Lidar, *Fault-tolerant quantum dynamical decoupling.* Phys. Rev. Lett. **95**, 180501 (2005)

[43] L. Jiang, J. S. Hodges, J. R. Maze, P. Maurer, J. M. Taylor, D. G. Cory, P. R. Hemmer, R. L. Walsworth, A. Yacoby, A. S. Zibrov, and M. D. Lukin, *Repetitive readout of a single electronic spin via quantum logic with nuclear spin ancillae.* Science **326**, 267–272 (2009)

[44] B. Fakler and J. P. Adelman, *Control of $K_{Ca}$ channels by calcium nano/microdomains.* Neuron **59**, 873–881 (2008)